Magnetic-field fluctuations around the radio galaxy 3C 31

R.A. Laing (ESO), A.H. Bridle (NRAO)

1 Introduction

Our knowledge of the structure and origin of magnetic fields in elliptical galaxies, groups and clusters is still rudimentary, but Faraday rotation of linearly-polarized radio emission can be used to probe the fields in ionized foreground gas. Here, we present an analysis of the magnetic-field fluctuations in the magnetoionic medium in front of the FR I radio galaxy 3C 31 ($z = 0.0169$) derived from rotation-measure (RM) fits to high-resolution polarization images. We first verify that the Faraday rotation is due primarily to a foreground medium. We then characterise its spatial statistics using a combination of structure-function and residual depolarization measurements. Finally, we present a three-dimensional simulation of a tangled magnetic field in the hot plasma and use this to fit the variation of RM fluctuation amplitude across the source.

2 Observed Faraday rotation and depolarization

Our analysis is based on VLA observations at 6 frequencies in the range 1.4 – 8.4 GHz with resolutions of 5.5 and 1.5 arcsec FWHM (Figs 1 and 2). We show images of normalized polarization gradient $p'(0)/p(0)$ from fits to $p(\lambda^2) = p(0) + p'(0)\lambda^2$, where $p(\lambda^2)$ is the degree of polarization at wavelength λ and a prime denotes differentiation with respect to λ^2 (e.g. Fig. 3 a – c). We also show RM images derived from fits to $\chi(\lambda^2) = \chi(0) + \mathrm{RM}\lambda^2$ at 4 – 6 wavelengths, where χ is the **E**-vector position angle (e.g. Fig. 3d –f).
The residual depolarization at 1.5 arcsec resolution is very small ($p'(0)/p(0) = -10\,\mathrm{m}^{-2}$ corresponds to a 5% reduction in polarization at 1.4 GHz) and the rotation is accurately proportional to λ^2, indicating almost completely resolved foreground rotation. There is a large asymmetry across the nucleus: the lobe with the brighter jet shows a much smaller RM fluctuation amplitude on all scales than the counter-jet lobe, qualitatively as expected from relativistic jet models [5].

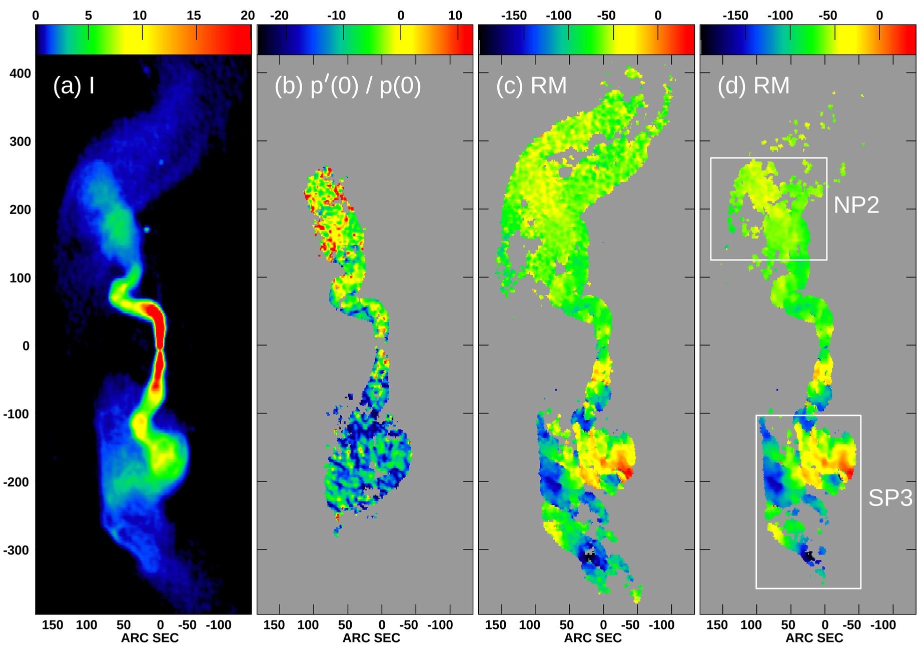

Figure 1: Images at 5.5 arcsec resolution. (a) Mean of 4 total-intensity images at frequencies from 1.4 – 1.7 GHz. (b) Normalized polarization gradient $p'(0)/p(0)$. (c) RM from a fit to 4 images at frequencies between 1.4 and 1.7 GHz. (d) As (c), but for 5 frequencies from 1.4 – 5.0 GHz.

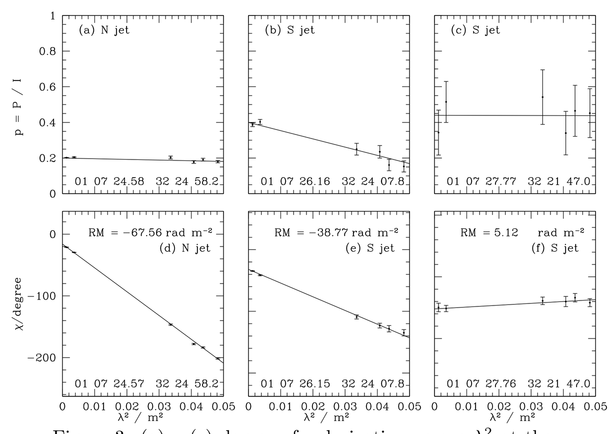

Figure 3: (a) – (c) degree of polarization versus λ^2 at the locations marked by the crosses in Fig. 2. (d) – (f) **E**-vector position angle versus λ^2 at the same locations.

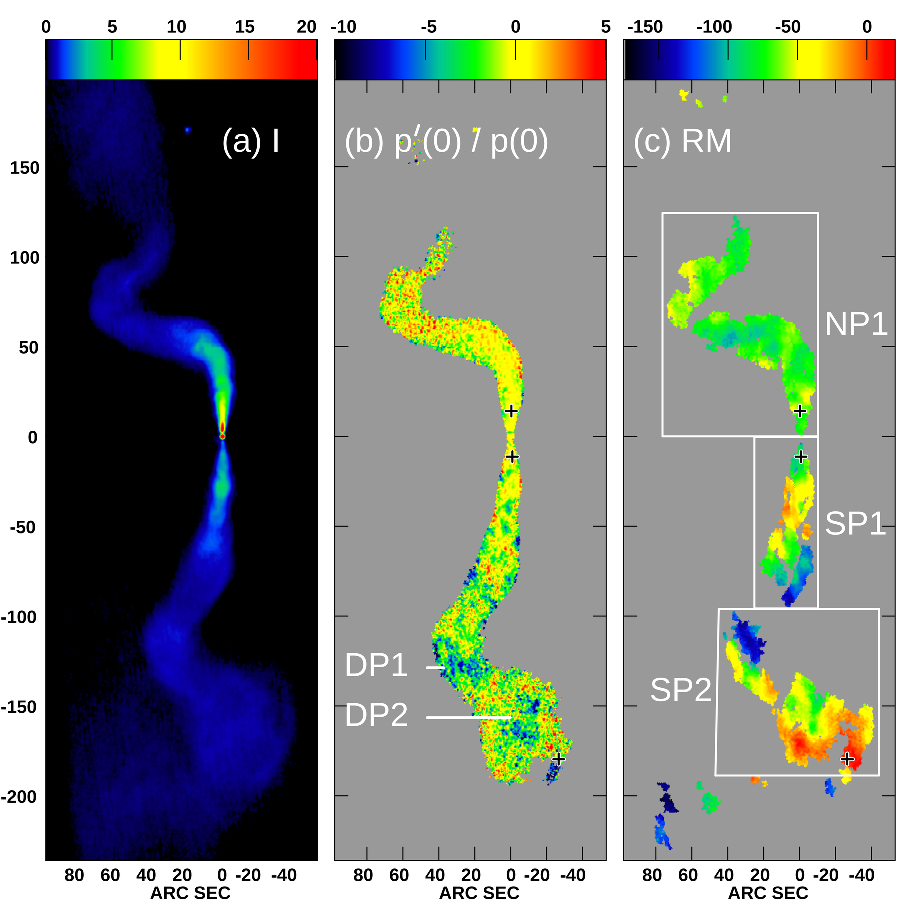

Figure 2: Images at 1.5 arcsec resolution. (a) Mean of 4 total-intensity images at frequencies from 1.4 – 1.7 GHz. (b) Normalized polarization gradient $p'(0)/p(0)$. (c) RM from a fit to 6 frequencies between 1.4 and 8.4 GHz using the PACERMAN algorithm [1].

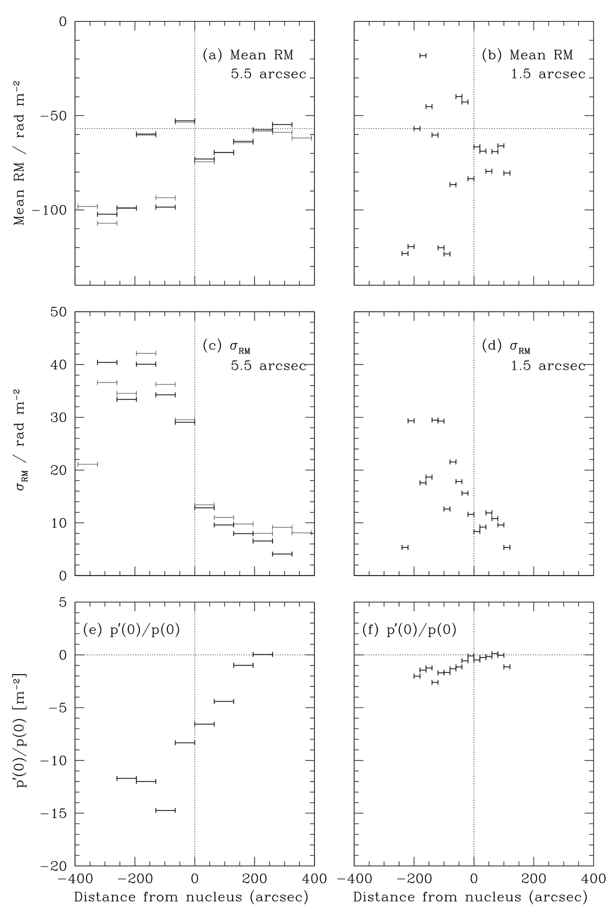

Figure 4: Profiles along the jet axis (positive distances are in the direction of the main jet and the vertical dotted lines show the position of the nucleus). Quantities are evaluated for boxes of length 65 arcsec along the axis for the 5.5 arcsec FWHM data (panels a, c and e) and 20 arcsec for the 1.5 arcsec FWHM data (panels b, d, f). (a) and (b) Mean RM, ⟨RM⟩. The horizontal dotted line is our best estimate for the Galactic rotation measure. (c) and (d) σ_{RM}, determined with respect to the local mean in the box. The values of σ_{RM} have been corrected to first order for the offset due to noise on the fit. (e) and (f) The mean value of the normalized polarization gradient $\langle p'(0)/p(0)\rangle$.

3 Analysis

We quantify the spatial variation of RM using the structure function $S(\mathbf{r}) = \langle[\mathrm{RM}(\mathbf{r}+\mathbf{r}') - \mathrm{RM}(\mathbf{r}')]^2\rangle$, where $\mathbf{r}$ and $\mathbf{r}'$ are separation vectors in the plane of the sky and $\langle\rangle$ denotes an average over $\mathbf{r}'$. Our data are consistent with isotropy, so we plot S as a function of scalar separation r for five regions of 3C 31 in Fig. 5. We start from a model RM power spectrum $\hat{C}(k)$, where k is the wave-number. Its Hankel transform is the RM autocorrelation function $C(r)$, and the structure function is $S(r) = 2[C(r) - C(0)]$. A novel feature of our analysis is that we include the effects of the observing beam explicitly (this can be done straightforwardly provided that the rotation across the beam is small, as is the case for our observations). Our data are consistent with a power spectrum which has the same form everywhere, but varying normalization. We have found two acceptable functional forms for the power spectrum: $\hat{C}(k) \propto k^{-2.35}$ with a high-frequency cut-off at $k = 0.5\,\mathrm{arcsec}^{-1}$ (a scale of 12 arcsec or 4 kpc) and a broken power-law form with $\hat{C}(k) \propto k^{-11/3}$ (as expected for Kolmogorov turbulence) for $k > 0.13\,\mathrm{arcsec}^{-1}$ and $\propto k^{-1.5}$ at larger scales. The predicted structure functions are very similar if the effects of the beam are included (Fig. 6). This may explain why earlier studies have come to different conclusions regarding the index of the power spectrum on the basis of RM analysis alone [8, 9, 7, 3]. **The cut-off power-law model with $\hat{C}(k) \propto k^{-2.35}$ predicts significantly less residual depolarization, however, in better agreement with our data for 3C 31.**
The easiest way to explain an asymmetry in RM fluctuation amplitude related to jet sidedness is to postulate that the rotation arises in a large-scale gas component surrounding the source – most plausibly the group-scale hot component. The asymmetry is then simply due to the differing path lengths through the gas to the approaching (brighter) and receding jets [5]. In order to model the asymmetry, we simulate the Faraday rotation from an isotropic, random magnetic field with a power spectrum corresponding to that derived from the RM structure-function analysis embedded in ionized gas with a smooth density distribution (cf. [7]). We first assume a spherically-symmetric density distribution with a core radius of 150 arcsec as fit to ROSAT data for the 3C 31 group by [4]. An example RM distribution for a radio source of negligible thickness inclined by 52° to the line of sight [6] is shown in Fig. 7 (d) – (f). The rms central magnetic field strength for this model is $\langle B_0^2\rangle^{1/2} = 0.21\,\mathrm{nT}$ (2.1 μG). The predicted RM distribution shows an asymmetry, but there is no sharp change at the nucleus and the profile falls too rapidly with distance on the counter-jet side. **The most plausible reason for the discrepancy is that the radio lobes have displaced the surrounding gas, which is therefore highly non-spherical.** Cavities in the X-ray-emitting gas associated with radio lobes are indeed observed in similar sources such as 3C 449 [1]. If we model the cavity as initially conical, with a half-opening angle of ≈55° within 100 arcsec of the nucleus and thereafter cylindrical, we can approximately reproduce the RM distribution (Fig. 7 g – i). Such a cavity would not have been apparent in the existing X-ray data [4], but should be detectable with XMM-Newton.

4 Structure functions and power spectra

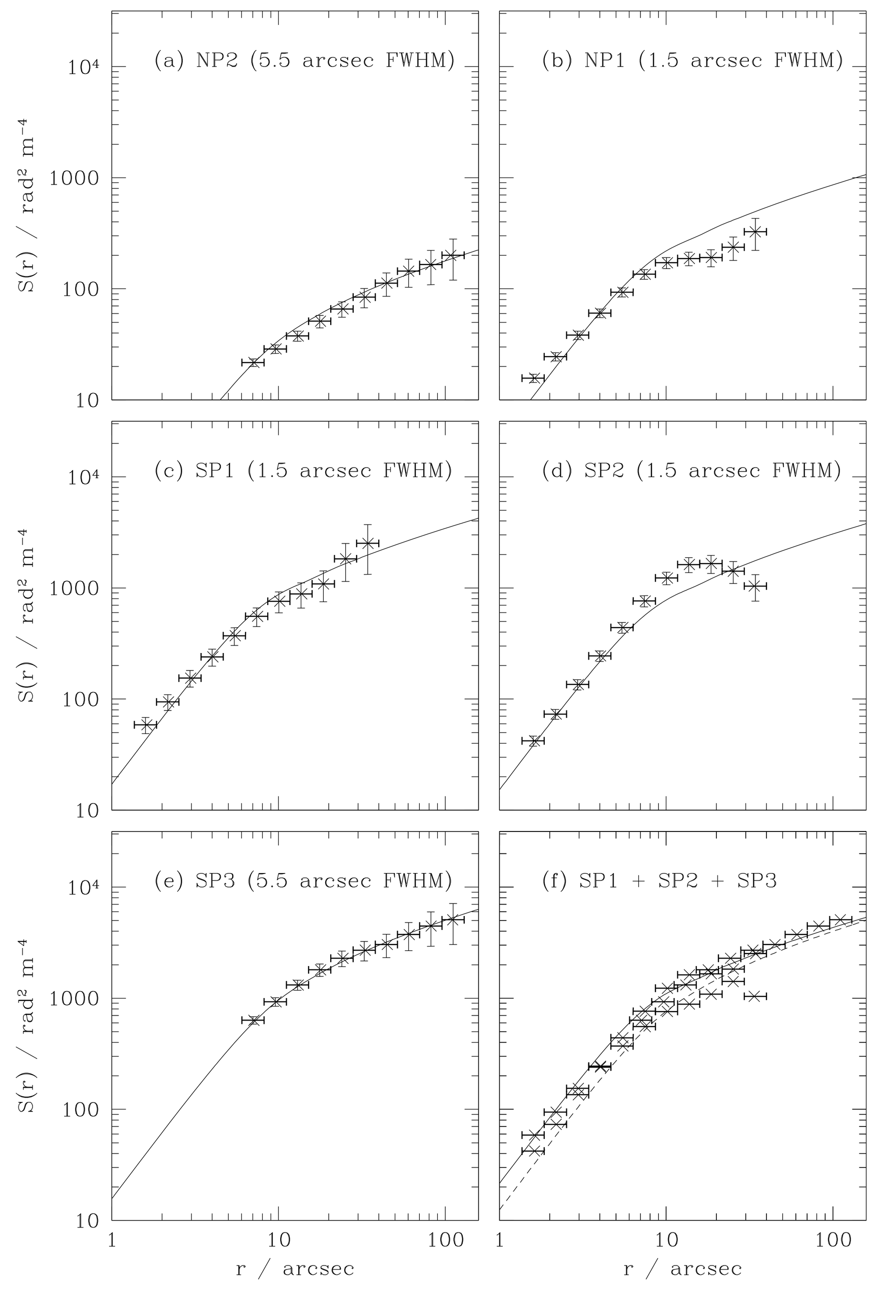

Figure 5: (a) – (e): plots of the RM structure function for the regions indicated in Figs 1 and 2. The horizontal bars represent the bin widths and the crosses the mean separation for data included in the bins. The curves are the predictions for the cut-off power law power spectrum described in the text, including the effects of the convolving beam. The error bars represent the rms variations for structure functions derived using multiple realisations of the model power spectrum on the observed grid of points for each region. Panel (f) shows the superposition of structure functions for al three regions in the S of the source. The full and dashed lines show model structure functions for FWHM 1.5 and 5.5 arcsec, respectively, with the same normalization.

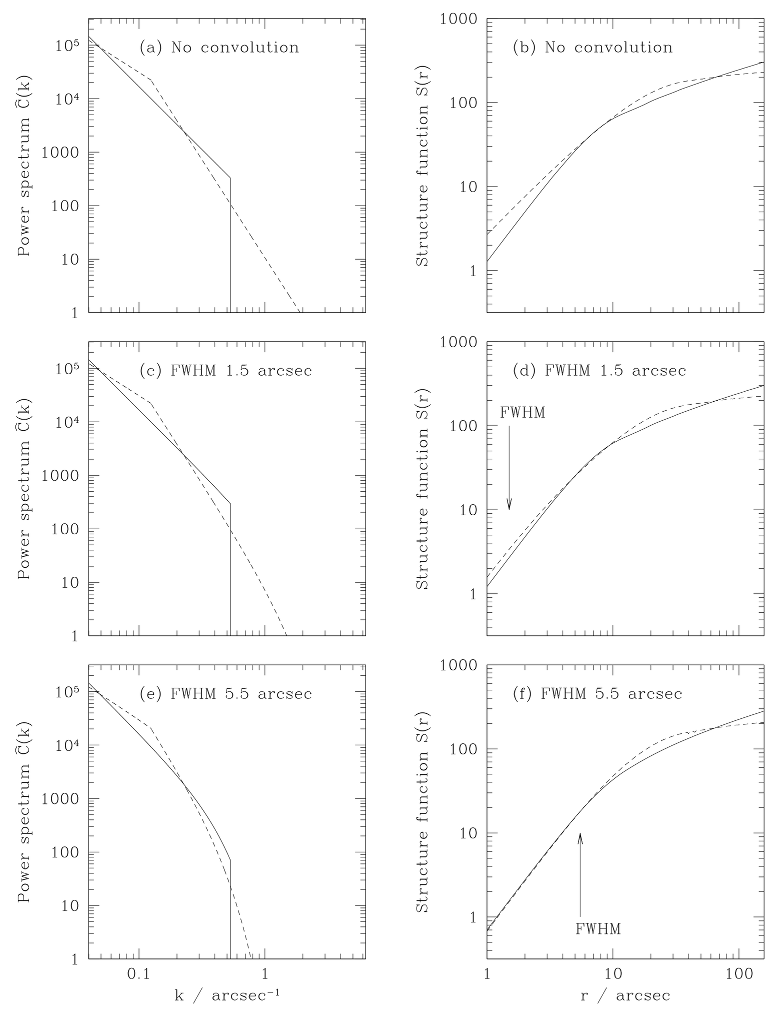

Figure 6: (a), (c), (e): the two model RM power spectra discussed in the text. Solid line, power law with index −2.35 and a high-frequency cut-off at $k = 0.5\,\mathrm{arcsec}^{-1}$. Dashed line: broken power-law with indices −11/3 and −1.5 and a break at $k = 0.13\,\mathrm{arcsec}^{-1}$. (b), (d), (f): structure functions computed for the power spectra in panels (a), (c) and (e), with the same line codes. (a) and (b) no convolution; (c) and (d) 1.5 arcsec FWHM convolving beam; (e) and (f) 5.5 arcsec FWHM convolving beam.

5 Three-dimensional simulations

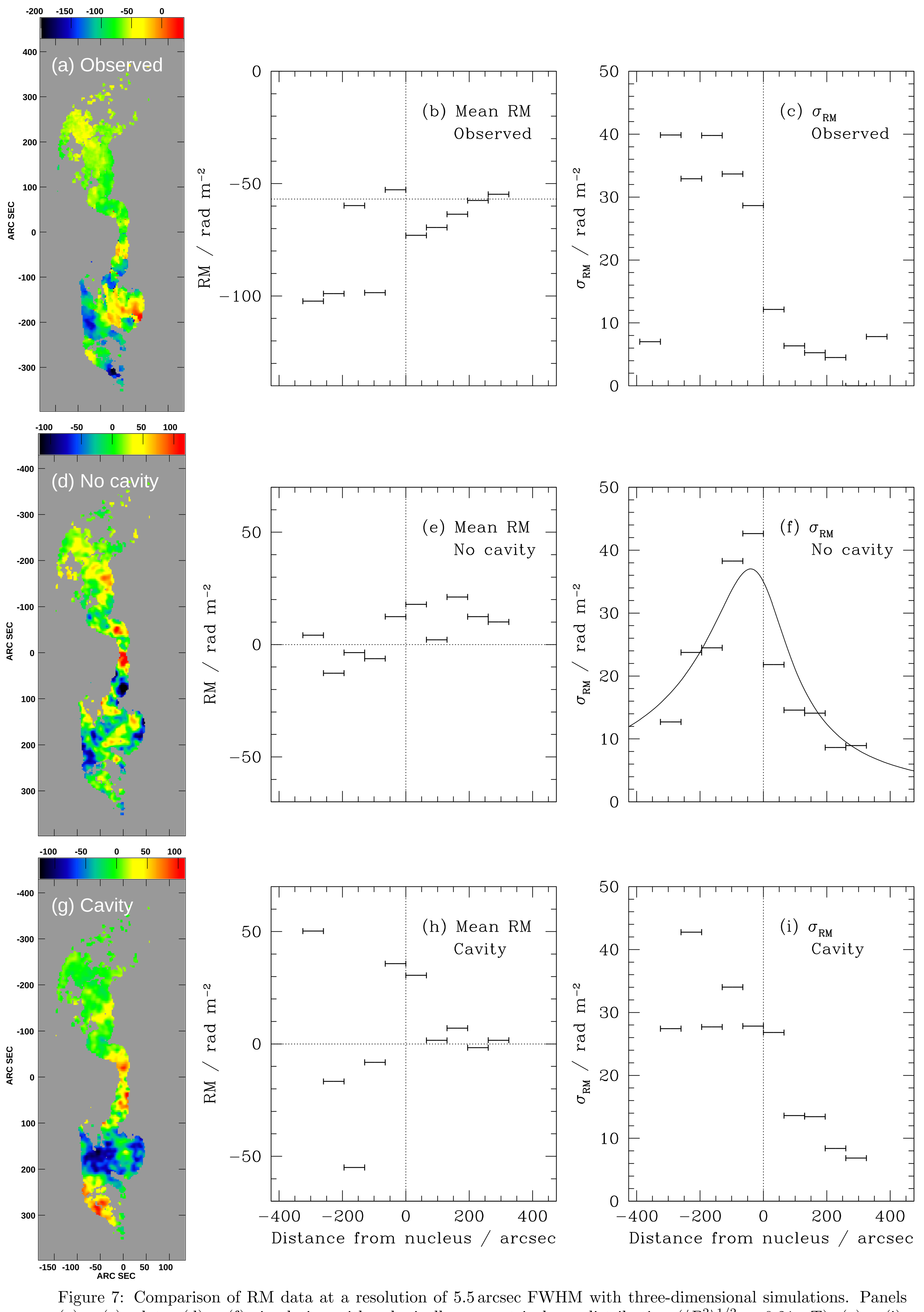

Figure 7: Comparison of RM data at a resolution of 5.5 arcsec FWHM with three-dimensional simulations. Panels (a) – (c): data; (d) – (f) simulation with spherically symmetrical gas distribution ($\langle B_0^2\rangle^{1/2} = 0.21$ nT); (g) – (i): simulation with cavity. (a), (d) and (g) show RM images. (b), (e) and (h) show mean RM values over boxes of length 65 arcsec along the jet axis, as in Fig. 4; (c), (f) and (i) the corresponding rms variations. The curve in panel (f) is the variation predicted by a single-scale model.

[1] Croston, J.H., Hardcastle, M.J., Birkinshaw, M., Worrall, D.M., 2003, MNRAS, 346, 1041

[2] Dolag, K., Vogt, C., Enßlin, T.A., 2005, MNRAS, 358, 726

[3] Govoni F., Murgia M., Feretti L., Giovannini G., Dolag K., Taylor G.B., 2006, A&A, 460, 425

[4] Komossa, S., Böhringer, H., 1999, A&A, 344, 755

[5] Laing, R.A., 1988, Nature, 331, 149

[6] Laing, R.A., Bridle, A.H., 2002, MNRAS, 336, 328

[7] Murgia, M., Govoni, F., Feretti, L., Giovannini, G., Dallacasa, D., Fanti, R., Taylor, G.B., Dolag, K., 2004, A&A, 424, 429

[8] Vogt, C., Enßlin, T.A., 2003, A&A, 412, 373

[9] Vogt, C., Enßlin, T.A., 2005, A&A, 434, 67